Performance Characterization of a Novel Thin Position-Sensitive Avalanche Photodiode for 1 mm Resolution Positron Emission Tomography

Jin Zhang, *Member, IEEE*, Angela M. K. Foudray, *Member, IEEE*, Peter D. Olcott, *Member, IEEE*, Richard Farrell, Kanai Shah, and Craig S. Levin, *Member, IEEE*

***Abstract*—We are developing dedicated breast and small animal positron emission tomography (PET) systems using scintillation detectors comprising $1 \times 1 \times 3$ mm^3 LSO crystals coupled to novel, extremely thin position-sensitive avalanche photodiodes (PSAPD). The detectors are placed in a novel configuration such that PSAPDs read the relatively large side faces of the crystals, with normally incident 511 keV photons entering parallel to the PSAPD surface. This configuration facilitates 1 mm^3 spatial resolution, directly measured photon interaction depth in 2 cm thick LSO, and $>90\%$ scintillation light collection efficiency. For this design, extremely thin (<300 μm) PSAPDs are required to achieve high crystal packing fraction for high intrinsic detection efficiency. The standard PSAPD (8×8 mm^2 active area) is packaged on a ceramic substrate, which is not compact enough for the desired detector configuration. The new PSAPD is packaged on a polyimid (Kapton) "flex" circuit with ~ 250 μm total thickness. This paper investigates whether the required modification to the PSAPD chip, packaging, and manufacturing processes lead to degraded performance for the thin device compared to the standard PSAPD. Electronically collimated coincidence measurements yielded an average intrinsic spatial resolution of 1.1 ± 0.1 mm FWHM, energy resolution of $10.8 \pm 0.6\%$ at 511 keV, and coincidence time resolution of 2.1 ± -0.2 ns FWHM for the standard PSAPD. The corresponding values measured for the thin PSAPD were very similar, 1.1 ± 0.1 mm FWHM, $10.9 \pm 0.7\%$, and 2.0 ± -0.3 ns, respectively. In summary, the new thin PSAPD allows us to attain the design specifications for the proposed ultra-high resolution, high sensitivity PET systems and performs comparable to the standard device.**

***Index Terms*—Avalanche photodiode, energy resolution, positron emission tomography, spatial resolution, time resolution.**

Manuscript received April 12, 2006; revised December 31, 2006. This work was supported in part by NIH-NCI under Grants R01 CA119056 and R21 CA098691, and by NIBIB under Grant R21/R33 EB003283.

J. Zhang was with the Department of Radiology and Molecular Imaging Program, Stanford University, Stanford, CA 94305 USA. He is now with PerkinElmer Optoelectronics, Santa Clara, CA 95054 USA (e-mail: jin.zhang@perkinelmer.com).

A. M. K. Foudray is with the Department of Radiology and Molecular Imaging Program, Stanford University, Stanford, CA 94305 USA and also with the Physics Department, University of California, San Diego, CA 92037 USA (e-mail: afoudray@stanford.edu).

P. D. Olcott and C. S. Levin are with the Department of Radiology and Molecular Imaging Program, Stanford University, Stanford, CA 94305 USA (e-mail: pdo@stanford.edu; cslevin@stanford.edu).

R. Farrell and K. Shah are with RMD Inc., Watertown, MA 02472 USA (e-mail: rfarrell@rmdinc.com; kshah@rmdinc.com).

Color versions of one or more of the figures in this paper are available online at http://ieeexplore.ieee.org.

Digital Object Identifier 10.1109/TNS.2007.894128

I. Introduction

HIGH resolution positron emission tomography (PET) systems have been developed for breast cancer imaging and small animal imaging studies [1]–[5]. Semiconductor photodetectors have been used in high resolution PET detector designs due to their higher quantum efficiency and better compactness compared to photomultiplier tubes (PMTs) [4]–[12]. To build a high resolution PET camera, the most common method is to use a discrete array of long and thin crystal rods with their narrow ends coupled to the photodetector array. However, this method has difficulties in extracting a sufficient fraction of the available scintillation light photons due to a poor aspect ratio for light collection, and the resulting light collection efficiency depends strongly on the photon interaction location within the crystal. A weak and varying scintillation light signal degrades spatial, energy, and temporal resolutions, and hence PET system performance.

We have proposed a PET detector configuration using an array of 1 mm lutetium oxyorthosilicate (LSO) scintillation crystals coupled "side-on" to silicon position sensitive photodiodes (PSAPD) with the PSAPD surface parallel to normal incident photons [6], [8], [9] as shown in Fig. 1(a). This configuration has shown promise for the desired performance specifications of 1 mm^3 intrinsic spatial resolution, $<12\%$ FWHM energy resolution, 2 ns FWHM coincidence time resolution, 2 cm effective LSO crystal thickness, and 3 mm directly measured photon depth-of-interaction (DOI) resolution, based on studies with a commercially available PSAPD [8], [9]. However, for PSAPDs coupled side-on to the crystals [Fig. 1(a)], in order to maintain the desired 70% crystal packing fraction goal for this new configuration, ultra-thin (<300 μm) PSAPDs are required [8], [9]. New, thin PSAPD chips, mounted on 50 μm thick polyimid (Kapton) "flex" circuit for bias and read-out, were fabricated for this purpose (RMD Inc., Watertown, MA). Fig. 1(b) shows pictures of the standard ceramic package and the new thin PSAPD mounted on a flex circuit. Fig. 1(c) shows a thin PSAPD coupled with 3×8 LSO crystal array, with half the crystals polished and the other half with ground surfaces (no inter-crystal reflector). The total thickness of the new flex PSAPD is ~ 250 μm. The PSAPD chips under study in this paper have a size of 11×11 mm^2 and a central sensitive area of 8×8 mm^2. In principle, modifying the chip and packaging as we have done can cause degraded device performance. In this paper, we present a performance comparison of the standard ceramic substrate mounted PSAPD with the new

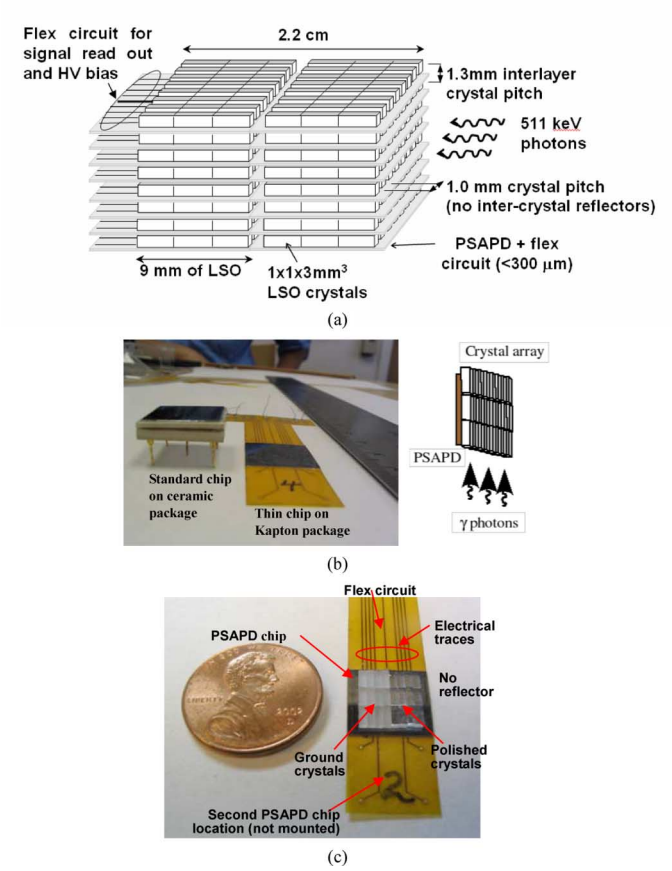

Fig. 1. (a) Schematic of "side-on" configuration of LSO crystals coupled to thin PSAPDs. (b) Picture of PSAPD with standard package and thin Kapton flex-circuit package; (c) Picture of a thin PSAPD coupled to a 3×8 LSO crystal array.

flex circuit mounted thin devices with regards to their energy resolution, coincidence time resolution, spatial resolution, and gain stability [13].

II. Materials and Methods

We tested energy resolution using flood irradiation (10 μCi Na-22 point source) on both a 4×3 array of $2 \times 2 \times 3$ mm^3 LSO crystals and an 8×3 array of $1 \times 1 \times 3$ mm^3 LSO crystals coupled side-on to the PSAPD array. For the 8×3 array of LSO crystals, we used half polished and half ground crystals to study how crystal surface treatment affects performance [see picture in Fig. 1(c)]. The array crystals were pressed together with no inter-crystal reflectors or gaps. The experimental setup is shown in Fig. 2(a). Signals from the four read-out channels at the corners of the PSAPD were amplified by Cremat (Watertown, MA) 110 preamplifiers and then further amplified by Ortec (Knoxville, TN) 855 shaping amplifiers. Then each of the four signals was split using a "T" connector, and one half was summed by an Ortec 433A module and the other half was fed into a National Instruments (Austin, TX) ADC digitizer card (PCI-6110) for data collection. The summed signal was used as the trigger to the digitizer. Data acquisition was controlled and collected in list mode by a National Instruments LabView program.

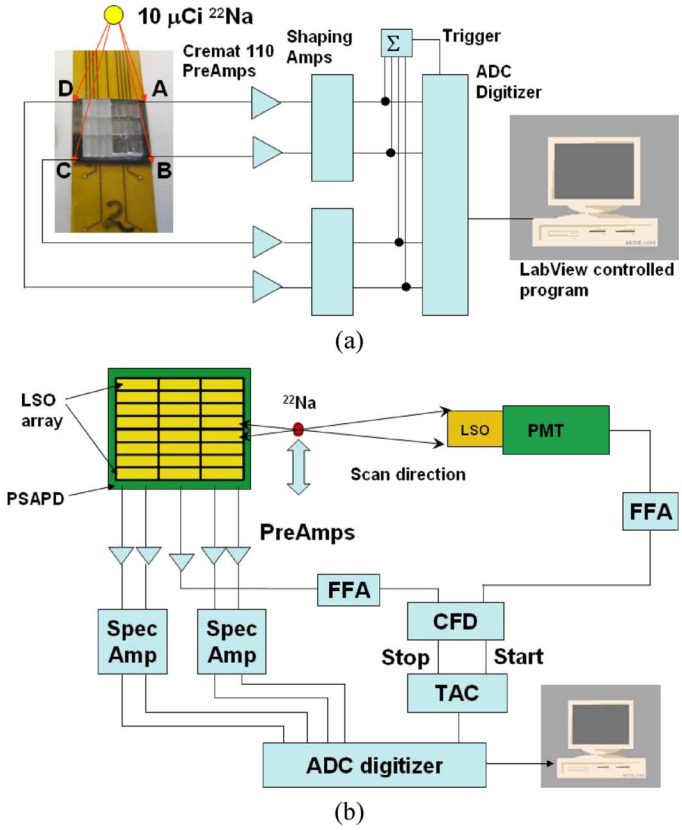

Fig. 2. Experimental setup for (a) crystal array flood image measurement and (b) coincidence time resolution and point spread function scan measurement.

Flood images were generated using signals from the four corner contacts of the PSAPD. Anger-type logic has been used to form the flood histogram before [8], which can be expressed as:

$$X = \frac{(A+B)-(C+D)}{A+B+C+D}$$
$$Y = \frac{(A+D)-(B+C)}{A+B+C+D}, \quad (1)$$

where A, B, C, and D are signals from the four corner channels of the PSAPD; X and Y are the coordinates of the photon interaction position on the detector surface. However, using Anger-type logic, flood images show a significant "pin-cushion" spatial non-linearity distortion [7], [8].

We have recently developed another positioning algorithm that calculates a scintillation light centroid using only two opposing diagonal corner signals [14], which can be simply expressed as:

$$X' = \frac{A-C}{A+C}$$
$$Y' = \frac{B-D}{B+D}, \quad (2)$$
$$X = X'\cos\left(\frac{\pi}{4}\right) + Y'\sin\left(\frac{\pi}{4}\right)$$
$$Y = Y'\cos\left(\frac{\pi}{4}\right) - X'\sin\left(\frac{\pi}{4}\right). \quad (3)$$

As only diagonal channels are used to determine X' and Y' in this new algorithm, we need to rotate the image by $\pi/4$ to

reorient it. The advantage of this algorithm is that it generates flood images with significantly reduced pin-cushion distortion and thus was used in this paper for flood image studies. The reason that this algorithm generates a much less distorted image comparing to traditional Anger-type logic is believed to be related to the more uniform charge sharing along the diagonal direction. Further finite-element simulation study on this behavior is under investigation and will be reported separately [15].

Fig. 2(b) shows the measurement setup for coincidence time resolution and spatial resolution (coincidence point spread function) measurements. We used a $2 \times 2 \times 3$ mm^3 LSO crystal coupled to a 1 cm diameter Hamamatsu photomultiplier tube (PMT) for the electronic collimation in the coincidence measurements. The signal from the PMT was used as the "start" channel for an Ortec 567 time-amplitude-converter/single channel analyzer (TAC/SCA) after it went through a fast filter amplifier (Ortec 579 FFA) and a quad constant-fraction discriminator (Ortec 935 CFD). The common (cathode) signal from the PSAPD was used as the "stop" channel to the TAC/SCA after FFA and CFD. The SCA signal was used as the trigger to the digitizer. For coincidence time resolution (CTR) measurements, the TAC output signal was recorded which allowed one to histogram the recorded time differences between the incoming PSAPD and PMT signals.

For the measurement of the coincidence point spread function (CPSF), the same LSO crystal coupled to a PMT used for the CTR measurement was mounted rigidly on a motor-driven stage with a 10 μCi ^{22}Na point source. This stage was scanned along the 8 crystal edge of the 8×3 LSO crystal array of $1 \times 1 \times 3$ mm^3 LSO crystals [Fig. 2(b)] with a 511 keV photon beam (beam size of about 0.6 mm) incident parallel to the PSAPD plane. The scanning step size was approximately 160 μm. As with the flood measurements there were no inter-crystal reflectors or gaps. Thus, the array covers a total area of 8×9 mm^2, which is slightly bigger than the actual 8×8 mm^2 active area of each PSAPD. Again, to evaluate the performance with different crystal surface finish, the 8×3 LSO array contained 12 crystals with polished surfaces on all sides, and the other 12 crystals with all ground surfaces. Signals from the four corner channels were recorded to generate the centroid of the interaction positions for each photon event in the crystal array.

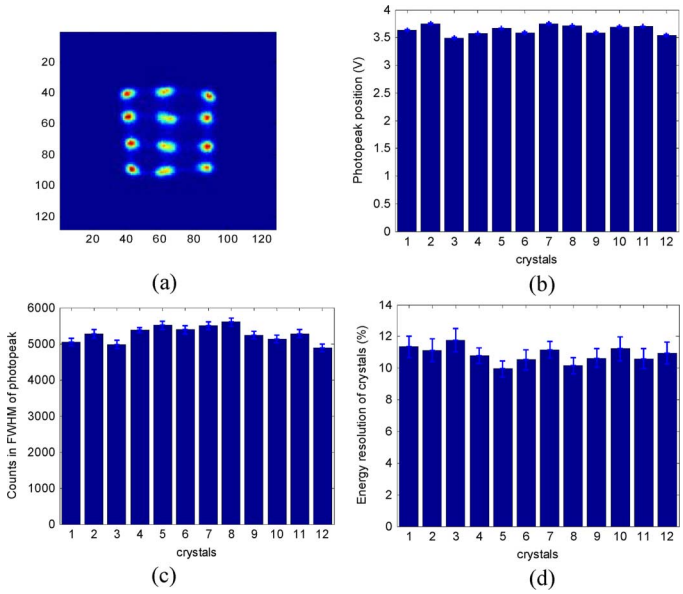

Fig. 3. Data from flood irradiation of the 3×4 array of $2 \times 2 \times 3$ mm^3 LSO crystals coupled to standard PSAPD. (a) Flood image, (b) bar plot of photopeak position; (c) bar plot of counts in FWHM; and (d) bar plot of FWHM photopeak energy resolution of individual crystals.

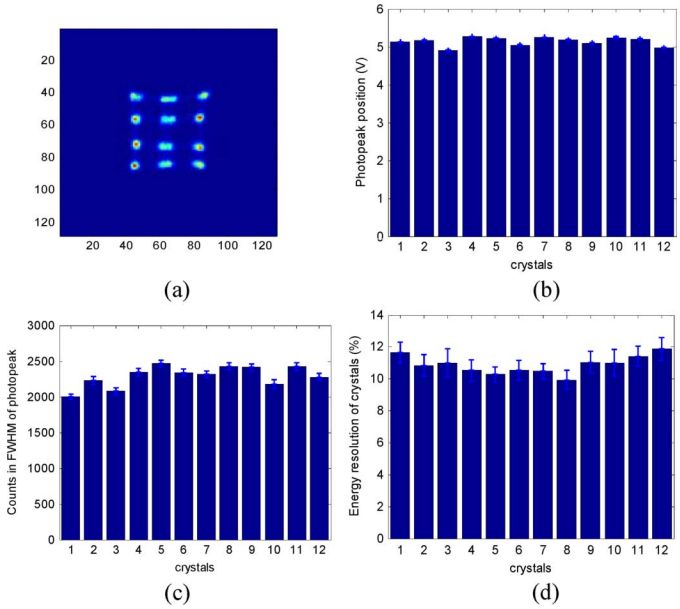

Fig. 4. Data from flood irradiation of the 3×4 array of $2 \times 2 \times 3$ mm^3 LSO crystals coupled to the new thin PSAPD. (a) Flood image; (b) bar plot of photopeak position; (c) bar plot of counts in FWHM; and (d) bar plot of FWHM photopeak energy resolution of individual crystals.

III. Results

A. Energy Resolution Measurement With 3×4 Array of $2 \times 2 \times 3$ mm^3 LSO Crystals

Fig. 3(a) shows the crystal flood histogram acquired with a 3×4 crystal array of $2 \times 2 \times 3$ mm^3 LSO crystals each coupled "side-on" to the standard PSAPD (with an 8×8 mm^2 sensitive area). The average photopeak position for the twelve crystals is 3.64 ± 0.01 volts [Fig. 3(b)]. The average counts in the FWHM of the photopeak are 5267 ± 108 [Fig. 3(c)]. The average crystal energy resolution (ER) at 511 keV is $10.9 \pm 0.6\%$, the best ER is $9.9 \pm 0.5\%$ and the worst ER is $11.8 \pm 0.7\%$, as shown in Fig. 3(d). For the thin flex circuit PSAPD, as shown in Fig. 4, the average photopeak position for the twelve crystals is 5.14 ± 0.01 volts [Fig. 4(b)]. The average photon counts in the FWHM of the photopeak are 2293 ± 50 [Fig. 4(c)]. Note that the flood source was further away than for the standard PSAPD measurement. The average ER at 511 keV for the 12 crystals is $10.9 \pm 0.7\%$ with the best ER of $9.9 \pm 0.6\%$ and the worst ER of $11.9 \pm 0.7\%$ [Fig. 3(d)]. It is observed that both the standard and new thin PSAPDs show comparable ER performance. The photon counts and photopeak positions are uniform for all twelve crystals. However, note that the new thin flex PSAPD

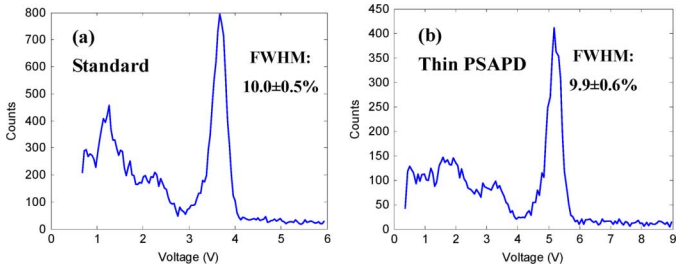

Fig. 5. Best Na-22 energy spectrum measured in $1 \times 1 \times 3$ mm^3 LSO coupled to the (a) standard and (b) new thin PSAPD.

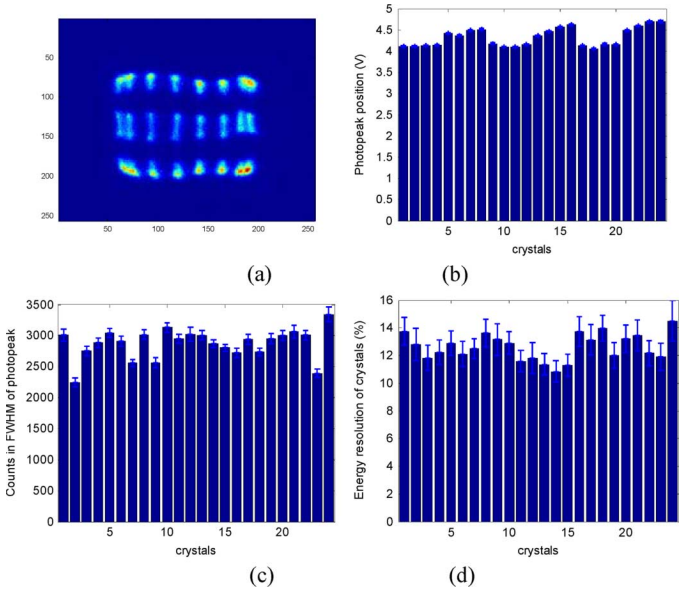

Fig. 6. Data from flood irradiation of the 3×8 array of $1 \times 1 \times 3$ mm^3 LSO crystals coupled to a standard PSAPD. (a) Flood image; (b) bar plot of photopeak position; (c) bar plot of counts in FWHM; and (d) bar plot of FWHM photopeak energy resolution of individual crystals.

has about 40% higher pulse height (photopeak position in energy spectrum) than the standard PSAPD. And the crystal locations appear more focused for the thin device. Fig. 5 shows the spectra with best ER for both PSAPDs.

B. Energy Resolution Measurement With 3×8 Array of $1 \times 1 \times 3$ mm^3 LSO Crystals

We also compared the standard and thin PSAPDs coupled to a 3×8 LSO array of $1 \times 1 \times 3$ mm^3 crystals. In order to study the effect of crystal surface finish on the performance, twelve of the 24 array crystals used had ground surfaces and the other twelve crystals had polished surfaces [see Fig. 1(c)]. The array crystals were pressed together with no inter-crystal reflectors or gaps. Thus the array covers a total area of 8×9 mm^2, which is slightly bigger than the actual 8×8 mm^2 active area of each PSAPD. Figs. 6 and 7 show the comparison of the flood positioning histogram, photopeak position, photon counts in FWHM, and ER of each $1 \times 1 \times 3$ mm^3 crystal for the standard and thin PSAPDs. For the standard PSAPD, the average photopeak position for the 24 crystals is 4.33 ± 0.02 volts [Fig. 6(b)]. The average counts in the FWHM of the photopeak are $2873 \pm$

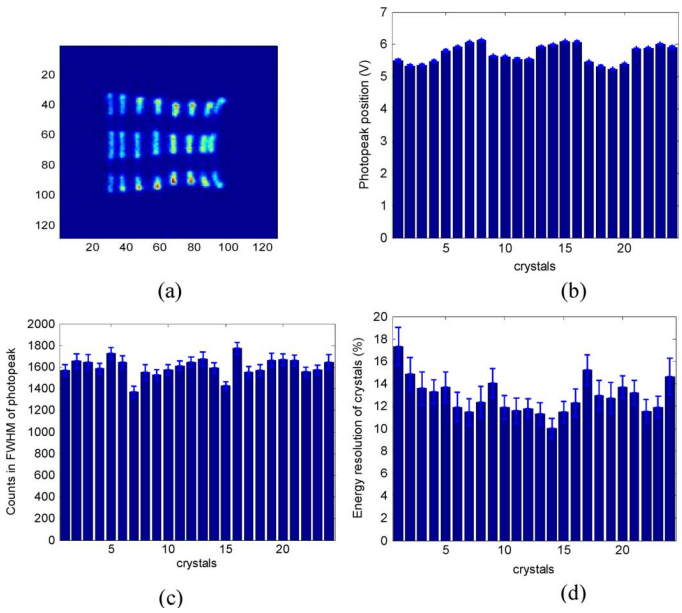

Fig. 7. Data from flood irradiation of the 3×8 array of $1 \times 1 \times 3$ mm^3 LSO crystals coupled to the new thin PSAPD. (a) Flood image; (b) bar plot of photopeak position; (c) bar plot of counts in FWHM; and (d) bar plot of FWHM photopeak energy resolution of individual crystals.

79 photons [Fig. 6(c)]. The average ER at 511 keV for the 24 crystals is $12.6 \pm 1.0\%$, with the best ER being $10.8 \pm 0.8\%$ and the worst $14.5 \pm 1.5\%$ for a crystal hanging off the edge of the sensitive area [Fig. 6(d)]. The $1 \times 1 \times 3$ mm^3 crystals hanging off the edge bring the average ER down below that quoted in Section 3.1 for the $2 \times 2 \times 3$ mm^3 crystals. For the new thin PSAPD, the average photopeak position for the 24 crystals is 5.71 ± 0.03 volts [Fig. 7(b)]. The average 511 keV photon counts in the FWHM of the photopeak are 1604 ± 54 photons [Fig. 7(c)]. Note again that the flood source was further away than for the standard device measurement. The average ER at 511 keV for the 24 crystals is $12.9 \pm 1.2\%$, with the best ER of $10.0 \pm 0.9\%$ and the worst ER of $17.4 \pm 1.7\%$ for a crystal hanging off the edge of the sensitive area [Fig. 7(d)]. Again we noticed that the new PSAPD has comparable ER but with about 32% higher pulse height than the standard PSAPD.

It is also of interest to compare the performance of the ground crystals and polished crystals. For the standard PSAPD, from Fig. 6, the average photopeak position, counts in FWHM and ER for the 12 ground crystals are 4.1 ± 0.2 volts, 2850 ± 80, and $12.7 \pm 1.0\%$ FWHM at 511 keV, respectively; and 4.5 ± 0.2 volts, $2896 \pm 77, 12.5 \pm 0.9\%$ FWHM for the 12 polished crystals, respectively. For the new thin PSAPD, from Fig. 7, the average photopeak position, counts in FWHM and ER for the 12 ground crystals are 5.5 ± 0.3 volts, 1606 ± 53, and $13.6 \pm 1.3\%$, respectively; and 6.0 ± 0.3 volts, $1601 \pm 54, 12.2 \pm 1.2\%$ for the 12 polished crystals, respectively. We thus observed that the polished crystals systematically had better ER and pulse height as compared to the ground crystals for both standard and new thin PSAPDs. The profile along the top, center and bottom eight crystal rows of the flood histograms for both standard PSAPD and thin PSAPD from Fig. 6 and 7 are plotted in Fig. 8. The new

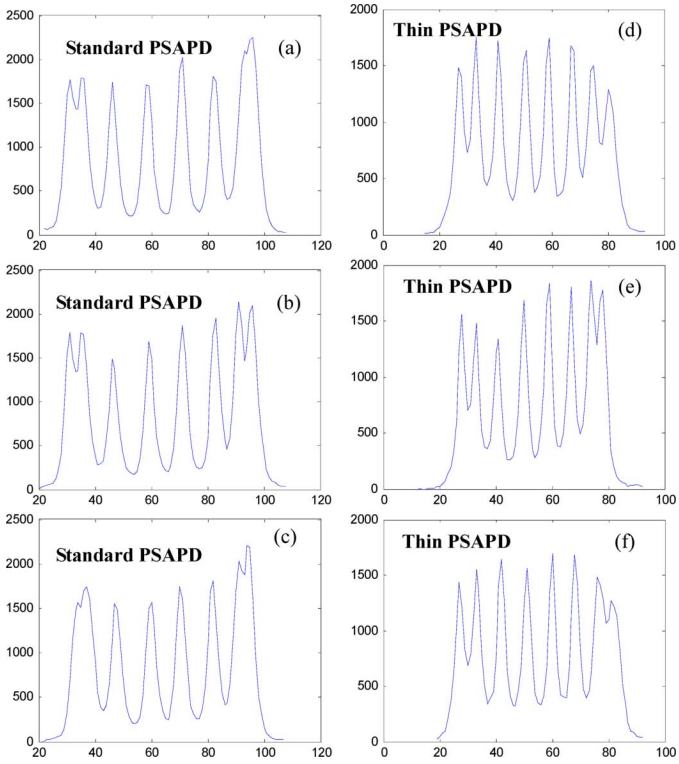

Fig. 8. 1-D profiles through the flood images in Fig. 6 for standard PSAPD (a, b, c) and in Fig. 7 for new PSAPD (d, e, f). (a, d) profile through upper row of 8 crystals, (b, e) center row of 8 crystals and (c, f) lower row of 8 crystals.

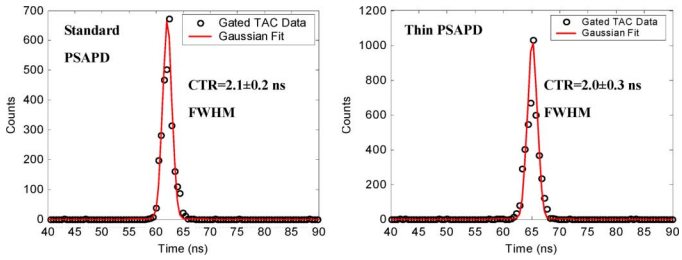

Fig. 9. Coincidence time spectra of the standard PSAPD (left) and flex mounted PSAPD (right) with FWHM resolution 2.1 ± 0.2 ns and 2.0 ± 0.3 ns, respectively.

PSAPD shows better crystal identification (peak-valley-ratio) than the standard PSAPD as will be discussed later.

C. Coincidence Time Resolution

Coincidence time resolution (CTR) was also measured for both PSAPDs. Fig. 9 shows that the measured CTRs of standard and thin devices, using an energy gate equal to the FWHM of the 511 keV photopeak, are 2.1 ± 0.2 ns and 2.0 ± 0.3 ns, respectively. Thus, the new thin flex-mounted PSAPD has comparable CTR to the ceramic packaged device.

D. Coincidence Point Spread Function

The sum of raw scanning data in Fig. 10 shows that the polished crystals have higher sensitivity than the ground crystals due to the slightly larger volume and higher light output, which tends to weight positioning toward those crystals. Notice that the left two columns of crystals (polished) are not clearly resolved by the standard PSAPD. However, the new flex PSAPD clearly

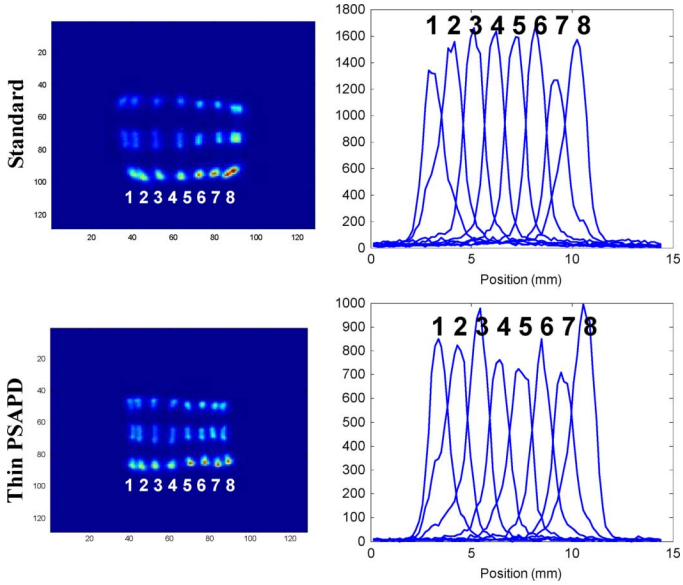

Fig. 10. Spatial resolution results of standard ceramic package PSAPD (top) and thin flex-mounted PSAPD (bottom). Left: Sum of raw data collected for point spread function measurements. Right: Point spread functions of the bottom 8 crystals in flood images, which are closest to the scanning source. The raw average FWHM of PSFs for the standard and flex PSAPDs is 1.3 ± 0.1 mm and 1.3 ± 0.1 mm, respectively. With 0.6 mm beam size deconvolution, the intrinsic spatial resolution is approximately 1.1 and 1.1 mm FWHM, respectively.

resolves the entire 3×8 crystal array in the raw sum image. The polished crystals in this coincidence PSF measurement also have better average ER of $12.5\% \pm 1.2\%$ vs. $14.7 \pm 1.3\%$ for ground crystals with the thin PSAPD. The CPSF of the eight crystals closest to the scanning source (bottom eight crystals in each raw summed image in Fig. 10) are also shown in Fig. 10. The average FWHM of raw CPSFs was 1.3 ± 0.1 mm for both the standard and flex PSAPDs. With photon beam size deconvolution, the intrinsic FWHM of CPSF for both the standard and thin PSAPDs is 1.1 ± 0.1 mm.

We also performed the spatial scan experiment along the 3-mm side of the polished and ground crystals to measure intrinsic photon depth resolution expected with the proposed detector configuration. Fig. 11 shows the CPSFs of the three polished or ground crystals along the 3 mm dimension. For the standard PSAPD, the average FWHMs of the CPSFs for the ground and polished crystals are 3.08 ± 0.04 mm and 2.96 ± 0.05 mm, respectively. For the new thin PSAPD, the average FWHMs of the point spread functions for the ground and polished crystals are 3.03 ± 0.05 mm and 2.97 ± 0.07 mm, respectively. The difference in CPSF for the ground and polished crystals is due to the slightly smaller dimensions of polished crystals. For both PSAPD devices, the CPSF is comparable.

E. Gain Stability Study

Gain stability of both standard and thin PSAPDs was also studied. We first measured the photopeak pulse height of the energy spectra and then measured it again after 20 hours with the PSAPD being continuously biased at -1740 volts. We noticed that the pulse heights of both PSAPDs were very stable, with a photopeak position fluctuation within 1.2% and 1.9% for the standard and thin PSAPD, respectively.

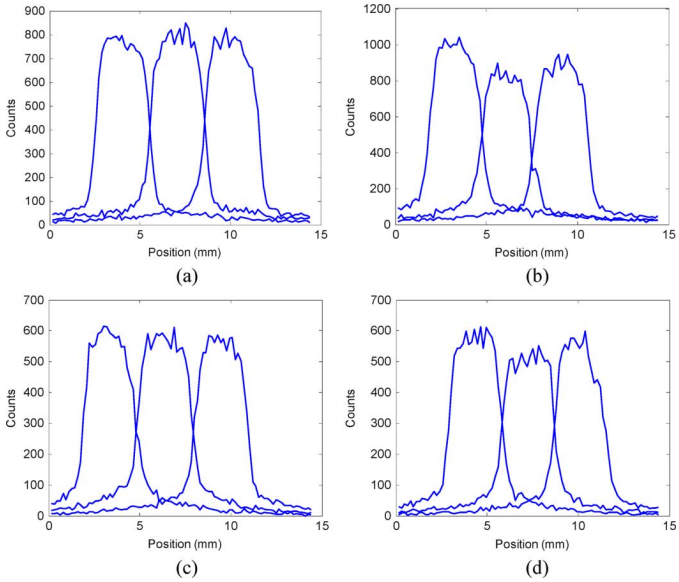

Fig. 11. Coincidence PSF of standard PSAPD for scan along the 3 mm crystal dimension for (a) ground crystals and (b) polished crystals and for thin flex PSAPD (c) along ground crystals and (d) along polished crystals.

IV. Discussion

As studied before, the new scintillation detector configuration (Fig. 1) with LSO crystals coupled side-on to the PSAPD surface achieves almost complete scintillation light collection [9]. This is because the light collection aspect ratio, which is defined as the ratio of the crystal readout area to the crystal length, has been significantly improved with this crystal-photodetector configuration. In this configuration, the light collection efficiency is also independent of where the photon interacts within the crystal. These properties of nearly complete and non-varying light collection efficiency are crucial to achieving the best intrinsic coincidence time, energy and spatial resolution performance available to this design.

The goal of this work is to develop ultra-high resolution PET cameras dedicated to breast cancer imaging and small animal imaging that achieve superior results in all important performance parameters for PET, including high intrinsic detection efficiency, and DOI resolution. In order to achieve high spatial resolution that is uniform throughout the useful FOV, we propose using $1 \times 1 \times 3$ mm^3 LSO crystal arrays which facilitate 3 mm directly measured photon DOI resolution in 2 cm thick LSO. For the proposed side-coupled design [Fig. 1(a)] the PSAPD had to be modified to be extremely thin and the standard ceramic substrate and package were replaced with a thin Kapton flex circuit. This paper studied the ER, CTR, and CPSF performance of the thin device and compared it to the standard ceramic mounted device. The results show that the new thin PSAPD has comparable ER, CTR and CPSF to the standard PSAPDs. The excellent ER and CTR values are very important for the PET camera to achieve excellent contrast resolution. State-of-the-art high resolution PET systems typically achieve $>20\%$ ER and >3 ns CTR [16] and a 60% energy window and 10 ns coincidence time window are typically used for data collection. With $\sim 12\%$ ER and ~ 2 ns CTR achieved with the new PSAPD configuration, one can use a narrower energy and time window (e.g., 24% and 4 ns, respectively) to significantly reduce the random and scatter coincidence event rates to improve the signal-to-noise ratio, contrast resolution and thus the imaging quality, while maintaining high photon count efficiency. Note that in order to better estimate the system CTR we still need to measure the time response contribution from the LSO-PMT channel alone or measure the CTR with two PSAPDs in coincidence.

State-of-the-art high-resolution PET systems have pushed the reconstructed spatial resolution to be below 2 mm at the center [16]. A key factor in system spatial resolution improvement is reduced crystal pixel size in detectors. With 1 mm LSO crystals, the proposed design has achieved an intrinsic CPSF of 1.1 mm FWHM and a DOI resolution of 3 mm FWHM. This interaction depth resolution is important to keep the system spatial resolution uniform throughout the FOV so that we may bring the detectors closer to the subject in order to achieve significantly improved photon sensitivity. A major goal is to build a high resolution PET system with the useful transaxial FOV equal to the physical detector gantry bore dimensions.

The new PSAPD also shows better crystal identification (peak-valley-ratio) than the standard PSAPD as shown in the flood images of Figs. 6 and 7. The profile along the top, center and bottom eight crystal rows is plotted in Fig. 8. We observed that the standard PSAPD has trouble resolving some of the crystals at the array edges. However, due to slightly larger sensitive area, the new thin PSAPD does not have this problem, as shown in Fig. 8. It is also noticed that the new PSAPD shows narrower and sharper crystal profiles in Fig. 8. The reason for some of these observed effects is not clear yet but it may be due to a significantly different, more favorable resistance distribution on the back side of the thin device.

V. Conclusion

The recently developed, thin, polyimid flex circuit mounted PSAPD has comparable spatial, energy and time resolutions to the ceramic packaged standard PSAPD and it also generates $\sim 40\%$ higher photopeak pulse height and superior crystal identification in flood positioning histograms. This extremely thin PSAPD, with ~ 1.1 mm FWHM intrinsic spatial resolution, $<13\%$ FWHM energy resolution, 2.0 ns FWHM coincidence time resolution, is essential for achieving high crystal packing fraction. In conclusion the new PSAPD achieves the design specifications required for the proposed ultra-high resolution PET systems under development.

Acknowledgment

The authors would like to thank colleagues Dr. G. Chinn and Dr. F. Habte for their input into this project.

References

[1] R. Freifelder and J. S. Karp, "Dedicated PET scanners for breast cancer," *Phys. Med. Biol.*, vol. 42, pp. 2463–2480, 1997.

[2] N. Doshi, Y. Shao, R. Silverman, and S. Cherry, "Design and evaluation of an LSO PET detector for breast cancer imaging," *Med. Phys.*, vol. 27, pp. 1535–1543, 2000.

[3] I. N. Weinberg, D. Beylin, V. Zavarzin, S. Yarnall, P. Y. Stepanov, E. Anashkin, D. Narayanan, S. Dolinsky, K. Lauckner, and L. P. Adler, "Positron emission mammography: High-resolution biochemical breast imaging," *Technol. Cancer Res. Treat.*, vol. 4, no. 1, pp. 55–60, 2005.

[4] W. M. Moses and J. Qi, "Instrumentation optimization for positron emission mammography," *Nucl. Instrum. Methods Phys. Res. A*, vol. A527, pp. 76–82, 2004.

[5] R. Lecomte, "Technology challenges in small animal PET imaging," *Nucl. Instrum. Methods Phys. Res. A*, vol. A527, pp. 157–167, 2004.

[6] C. S. Levin and E. J. Hoffman, "Investigation of a new readout scheme for high resolution scintillation crystal arrays using photodiodes," *IEEE Trans. Nucl. Sci.*, vol. 44, no. 3, pp. 1208–1213, Jun. 1997.

[7] K. S. Shah, R. Farrell, R. Grazioso, E. S. Harmon, and E. Karplus, "Position-sensitive avalanche photodiodes for Gamma-ray imaging," *IEEE Trans. Nucl. Sci.*, vol. 49, no. 4, pp. 1687–1692, Aug. 2002.

[8] C. S. Levin, A. M. K. Foudray, P. D. Olcott, and F. Habte, "Investigation of position sensitive avalanche photodiodes for a new high-resolution PET detector design," *IEEE Trans. Nucl. Sci.*, vol. 51, no. 3, pp. 805–810, Jun. 2004.

[9] C. S. Levin, "Design of a high-resolution and high-sensitivity scintillation crystal array for PET with nearly complete light collection," *IEEE Trans. Nucl. Sci.*, vol. 49, no. 5, pp. 2236–2243, Oct. 2002.

[10] K. C. Burr, A. Ivan, J. LeBlanc, S. Zelakiewicz, D. L. McDaniel, C. Kim, A. Ganin, K. Shah, R. Grazioso, R. Farrell, and J. Glodo, "Evaluation of a position sensitive avalanche photodiode for PET," *IEEE Trans. Nucl. Sci.*, vol. 50, no. 4, pp. 792–796, Aug. 2003.

[11] P. A. Dokhale, R. W. Silverman, K. S. Shah, R. Grazioso, R. Farell, J. Glodo, M. A. MeClish, G. Entine, V.-H. Tran, and S. R. Cherry, "Performance measurements of a depth-encoding PET detector module based on position-sensitive avalanche photodiode read-out," *Phys. Med. Biol.*, vol. 49, pp. 4293–4304, 2004.

[12] B. J. Pichler, B. K. Swann, J. Rochelle, R. E. Nutt, S. R. Cherry, and S. B. Sigel, "Lutetium oxyorthosilicate block detector readout by avalanche photodiode arrays for high resolution animal PET," *Phys. Med. Biol.*, vol. 49, pp. 4305–4319, 2004.

[13] C. S. Levin, J. Zhang, A. M. K. Foudray, R. Farrell, P. D. Olcott, M. McClish, F. Habte, and K. S. Shah, "A thin position sensitive avalanche photodiode for ultra-high resolution PET," presented at the 2004 IEEE Nuclear Science Symp. and Medical Imaging Conf., Abstract #M5-130, Book of Abstracts, p. 164, IEEE Nuclear and Plasma Science Society.

[14] J. Zhang, P. D. Olcott, and C. S. Levin, A New Algorithm for the Event Positioning with Position-Sensitive Scintillation Detectors (patent pending).

[15] P. D. Olcott, J. Zhang, C. S. Levin, F. Habte, and A. M. K. Foudray, "Finite element model based spatial linearity correction for scintillation detectors that use position sensitive avalanche photodiodes," in *Proc. IEEE Nuclear Science Symp. Conf. Rec.*, 2005, vol. 5, pp. 2459–2462.

[16] Y. C. Tai, A. Ruangma, D. Rowland, S. Siegel, D. F. Newport, P. L. Chow, and R. Laforest, "Performance evaluation of the microPET focus: A third-generation microPET scanner dedicated to animal imaging," *J. Nucl. Med.*, vol. 46, no. 3, pp. 455–463, Mar. 2005.